Journal of Power Sources 196 (2011) 2644–2649

Contents lists available at ScienceDirect

Journal of Power Sources

journal homepage: www.elsevier.com/locate/jpowsour

Out-of-phase thermo-mechanical coupling behavior of proton exchange membranes

Xu Chen*, Lei Yan, Zhenfeng Wang, Dan Liu

School of Chemical Engineering and Technology, Tianjin University, 92 Weijin Road, Nankai district, Tianjin 300072, China

ARTICLE INFO

Article history:
Received 14 September 2010
Received in revised form
11 November 2010
Accepted 12 November 2010
Available online 19 November 2010

Keywords:
Proton exchange membrane (PEM)
Fuel cell
Thermo-mechanical coupling
History-dependent
Thermal stress hysteresis

ABSTRACT

The thermal effects and mechanical effects on the durability of proton exchange membranes (PEMs) have been studied extensively in the literatures. However researches on the thermo-mechanical coupling behavior of PEMs are very limited. In this study, the interaction of mechanical and thermal effects in Nafion® NRE-212 was investigated using experimental methods. The thermo-mechanical coupling experiments were conducted following the in-phase proportional loading path, where the maximum/minimum mechanical loads and temperatures occur simultaneously and out-of-phase non-proportional rectangular loading paths where a phase difference of 90° existed between thermal and mechanical loads. During the creep processes under a variable temperature in out-phase profiles, the creep strain was found to be history-dependent in the membrane. The effect of initial temperature on the creep was significant in the first cycle. Moreover, temperature cycles were applied as thermal loading conditions and the history-dependence was also observed for thermal stresses. The maximum thermal stress did not occur at the lowest temperature.

1. Introduction

The performance of proton exchange membranes (PEMs) plays a very important role in the fuel cell applications and its durability impacts on battery life directly [1–3]. Currently, for mechanical side of the study, the cyclic mechanical stresses of the constrained membranes resulted from the hygrothermal cycles in fuel cell environment under operating conditions are believed to contribute to failure of PEMs [4,5]. The demanding automotive duty cycle of proton exchange membranes fuel cells (PEMFCs) requires the membrane to survive extensive temperature cycles and mechanical loadings [6–8]. These two types of loads are imposed at the same time very often. The thermo-mechanical coupling will lead to the nonlinear deformations and variation of the stresses in the polymers [9,10] and the temperature changes during mechanical tests could dramatically affect the stress–strain behavior of the membrane [11]. To our best knowledge, limited literatures have focused on the responses of PEMs under thermo-mechanical coupling loading conditions. In this work, the effect of thermo-mechanical coupling on mechanical properties of PEMs was investigated through a series of experiments following various loading paths and the thermal stresses in the membranes were also studied via temperature cyclic loading.

2. Materials and experimental procedure

The material tested was perfluorosulfonic acid (PFSA) with the trade name Nafion® NRE-212 developed and manufactured by DuPont. The original sample was a wide membrane with thickness of 0.0503 mm at first and then processed into rectangular strips of 25 mm × 5 mm according to ASTM standards [12].

The experiments were all conducted on a dynamic mechanical analysis (DMA-Q800, TA Instrument) and a film tension clamp was used (Fig. 1). The temperature sensor of the DMA-Q800 instrument was located in the furnace of the DMA close to the testing specimen installed in the tension clamp. Three thermo-mechanical coupling loading paths were applied on the membrane: a proportional path, and rectangular paths in counter-clockwise (CCW) direction and clockwise (CW) direction. The applied coupling loading histories are as shown in Fig. 2. In the proportional loading path, the thermal load and the mechanical load were applied to the specimen in phase (Fig. 2(a)). The range of loading temperature is from −30 °C to 55 °C with a changing rate of ±8 °C min^{-1}. The mode of mechanical loading is stress-control, and the stress range is from 0 MPa to 8 MPa with a rate of ±2 MPa min^{-1}. Because DMA was designed with single-channel control mode, only one type of the loads can be applied. The experiments were carried out with a discrete approach by dividing the loading process into many small discrete time periods. Only one type of load was applied at a certain period of time when the other was held constant. The two types of loads were imposed alternately. This approach provided

* Corresponding author. Tel.: +86 22 27408399; fax: +86 22 27403389.
E-mail address: xchen@tju.edu.cn (X. Chen).

0378-7753/$ – see front matter © 2010 Elsevier B.V. All rights reserved.
doi:10.1016/j.jpowsour.2010.11.071

Fig. 1. The film tension clamp.

a good approximation for our predetermined proportional path where maximum/minimum mechanical loads on the specimen and temperatures occur simultaneously.

In the cases of rectangular paths of thermo-mechanical coupling loading, the waveforms of the temperature and the stresses are both trapezoidal. For 90° phase difference between the thermal and mechanical loads, a trapezoidal history can result in a rectangular loading path which means a rectangular trace can be created in

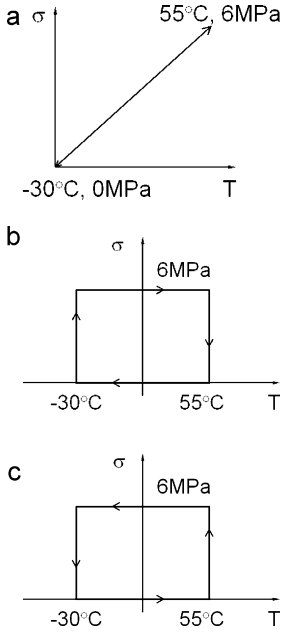

Fig. 2. The three kinds of loading paths: (a) proportional loading, (b) rectangular path loading (CCW) and (c) rectangular path loading (CW).

Table 1
The thermo-mechanical coupling case of CCW path.

Step	Temperature (°C)	Stress (MPa)
1	55	0–6
2	55 to −30	6
3	−30	6–0
4	−30 to 55	0

Table 2
The thermo-mechanical coupling case of CW path.

Step	Temperature (°C)	Stress (MPa)
1	55(25[a]) to −30	0
2	−30	0–6
3	−30 to 55	6
4	55	6–0

[a] The initial temperature of the first cycle is 25 °C.

the stress–temperature plot, as illustrated in Fig. 2(b) and (c). The thermal load was applied at a certain rate with a fixed mechanical load, and then the mechanical load was applied with a fixed thermal load until the whole cycle was completed. It is noteworthy that the rectangular loading path can be divided into two kinds of loading modes. One is called CCW rectangular loading path by elevating temperature first as shown in Fig. 2(b). The other is called CW rectangular loading path by reducing the temperature first as shown in Fig. 2(c). The temperature range of rectangular path loading is −30 °C to 55 °C with the changing rate of ±8 °C min^{-1}. The loading mode of mechanical load is stress control with the stress range of 0–6 MPa and rate of ±2 MPa min^{-1}. All the steps are shown in Table 1 for CCW loading path and Table 2 for CW loading path.

The temperature cyclic experiment was also conducted in this paper. Only thermal loads were imposed on the specimen repeatedly. A small strain (1%) was hold in the specimen first. After the equilibration of the stresses caused by such a small strain, temperature changes were applied. The range of temperature is from −30 °C to 85 °C at the rate of ±10 °C min^{-1}.

3. Results and discussion

3.1. Proportional loading tests

The resulting strain response for the proportional thermo-mechanical loading path is indicated in Fig. 3. As plotted, the stress

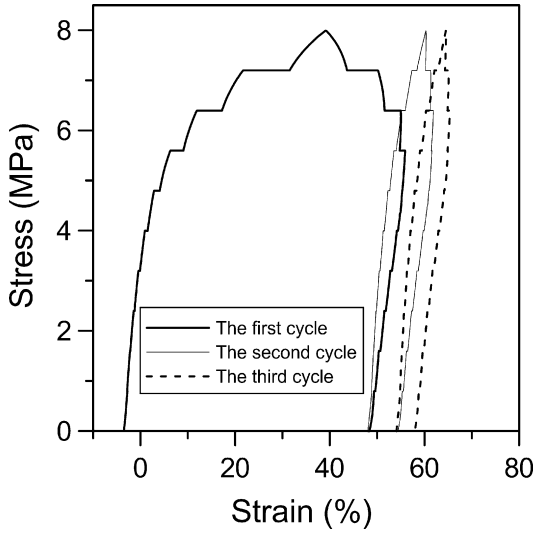

Fig. 3. The stress–strain response of proportional loading.

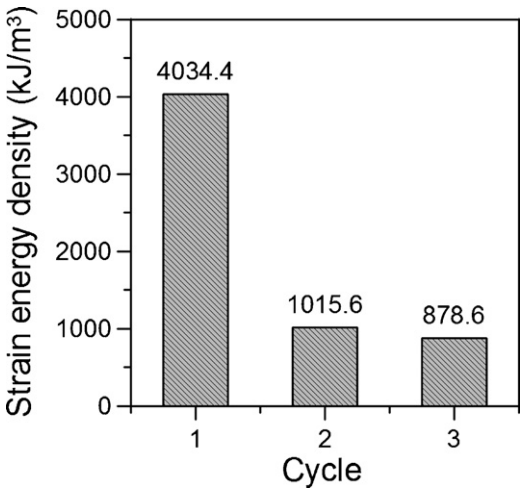

Fig. 4. The strain energy density vs. cycle number.

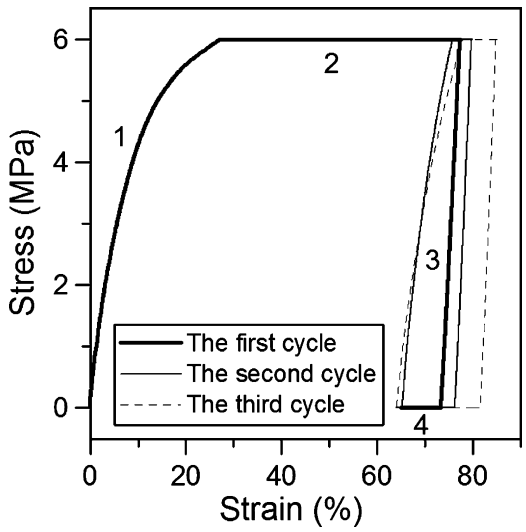

Fig. 5. The stress–strain response of CCW rectangular path loading.

changed step by step. During each step when stress was constant, the thermal load was imposed. This specific loading profile can be seen as a combination of stress controlled ratcheting test and creep tests. The mean stress in the specimen of the cyclic mechanical loading was 4 MPa. During each temperature loading period, the increases of strain were actually resulted from creep as stresses were held constant in the membrane and the thermal expansion caused by temperature changes. The total increase of strain was more pronounced in the first cycle than those in the second and the third cycle. To be noticed, starting from the second cycle, the creep strain was smaller than that in the first. The total strain increase of each cycle is defined as ε_i, where the subscript i is the number of each loading cycle. Then for each cycle of the test, $\varepsilon_1 = 51.12\,\%$, $\varepsilon_2 = 6.01\,\%$, and $\varepsilon_3 = 3.72\,\%$. The strain was significantly reduced after the first cycle and tended to reach equilibrium in subsequent cycles.

In order to investigate the damage of specimen under cyclic loading, the area surrounded by the stress and strain is calculated by integration and defined as strain energy density, ΔW^{d}. The changes of strain energy density reflect the level of saturation of tensile strains. As already analyzed, the strain of specimen is composed of two parts: one is the accumulation of plastic strain caused by cyclic stresses; the other is the creep strain in each cycle. It is believed that the strain caused by plastic accumulation under tension is close to its saturation when the variation of strain energy density is close to zero or the stress–strain curves of two adjacent cycles stays basically the same. The calculation gave $\Delta W_1^{\mathrm{d}} = 4034.4\ \ \mathrm{kJ\ \ m^{-3}}$; $\Delta W_2^{\mathrm{d}} = 1015.6\ \ \mathrm{kJ\ \ m^{-3}}$ and $\Delta W_3^{\mathrm{d}} = 878.6\ \ \mathrm{kJ\ \ m^{-3}}$. As the trend shown in Fig. 4, the membrane rapidly reached an equilibrium state after the first cycle when the specimen was tested in the case of interaction of thermal load and mechanical load.

3.2. Rectangular path loading tests

The stress–strain curve under CCW loading path is shown in Fig. 5. In each cycle, the experiment was carried out from the starting point of tensile loading at 55 °C, and then went through a cooling process with constant stress, an unloading process at a fixed temperature, and heating with zero stress in the specimen back to 55 °C. The temperature–strain curve is shown in Fig. 6 and four steps of the test are pointed out respectively. As analyzed along with Fig. 5, the step 1 was a stress ramp process and the ramping modulus of the second and the third cycles were higher than that of the first cycle. The step 2 was a constant-stress cooling process from 55 °C to −30 °C. The creep strains of the three cycles were 50.04%, 13.41% and 7.01% respectively showing a trend of gradual decrease with increasing number of cycles. The creep quickly finished the primary stage where the creep strain rate was relatively high and started entering the steady state with a low creep strain rate. Step 3 was an unloading process at the low temperature, −30 °C. The unloading moduli in three cycles were 151.1 MPa, 171.4 MPa and 182.4 MPa separately. The three moduli were very close to each other under low temperature unloading and the differences among them were farther smaller than the difference of modulus under high temperature loading process. The step 4 was a heating process with zero stress and the temperature rose from −30 °C to 55 °C at the rate of 8 °C min^{-1}. Within this zero stress step, the strain was reduced mainly by the recovery of the creep. The strain accumulated in the previous steps was recovered in this step. As the temperature went up, the creep compliance of the membrane increased and the level of recovery was declined.

For these three cycles, the strain energy density was 4378.9 kJ m^{-3}, 1333.1 kJ m^{-3}, 1087.6 kJ m^{-3} separately and was plotted against number of cycles in Fig. 7. As can be seen in the plot, the strain energy density equilibrated rapidly.

As the loading conditions shown in Table 2, CW rectangular path of loading started from cooling the air down to −30 °C first. The stress–strain curve and the strain–temperature curve are shown

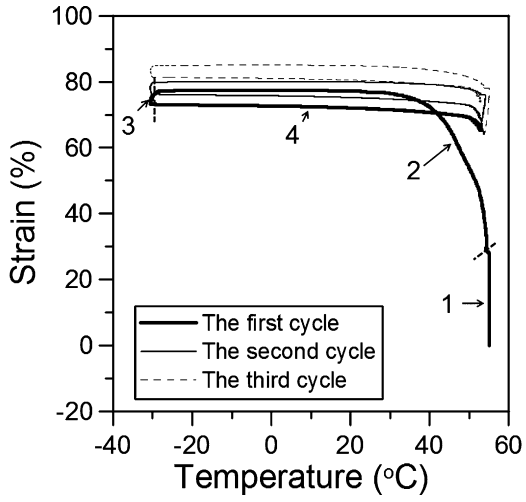

Fig. 6. The curve of the relation between strain and temperature. The step number was appointed to corresponding part of the curve for the first cycle.

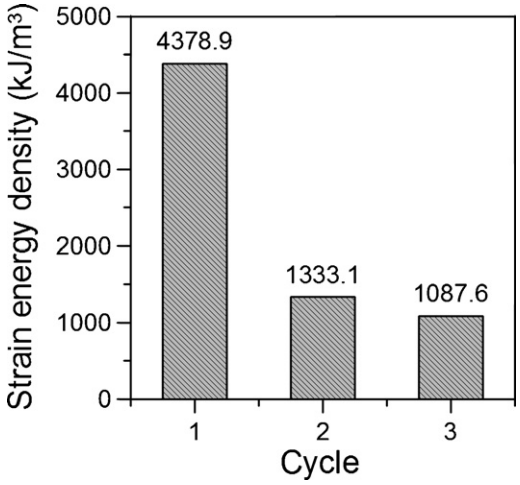

Fig. 7. The strain energy densities for loading cycles for CCW path.

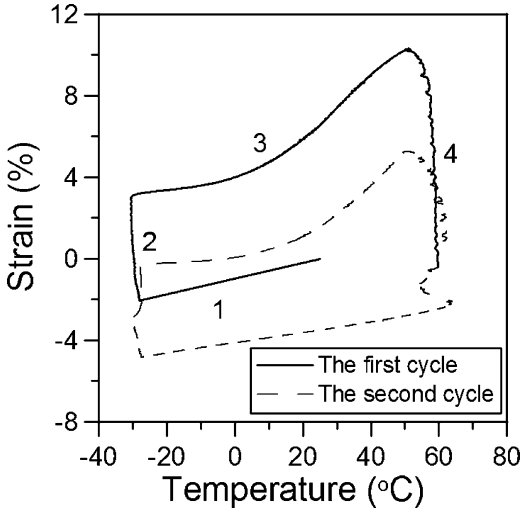

Fig. 9. The curve of the relation between strain and temperature of CW path.

in Figs. 8 and 9. Different from CCW loading, the unloading step in CW path was performed at high temperatures and the loading step was at low temperatures. Between first and second cycle, the change of unloading modulus is pronounced. On the contrary the change of loading modulus, E, between two cycles is comparatively small. E of the first and second cycle are 118.6 MPa and 137.1 MPa respectively. Summarizing the results of CCW and CW paths, we noticed that at low temperatures the change of modulus vs. cycles was small and the modulus increased with increasing cycles. It can be seen from the stress–strain curves that the specimen is almost completely elastic at the temperature well below the freezing point of water 0 °C and the β transition around 20 °C assigned as the glass transition temperature of the Nafion® non-ionic matrix [13]. The β transition related to chain motions of amorphous fluorocarbon units [14]. The ice formation from the free water and the freezable water content in the membrane could also increase the elastic modulus of Nafion® [15]. At the temperature above β transition, herein 55 °C, under tensile loading and unloading conditions, the material showed more nonlinearity.

The variable temperature creep steps at 6 MPa in both rectangular out-phase paths was compared in Fig. 10. For the case of CW path, the temperature rose from −30 °C to 55 °C and the creep strains in the first and the second cycle were 7.32% and 5.71% separately. For the case of CCW loading path, the temperature decreased from 55 °C to −30 °C and the creep strains for the first two cycles were significantly higher than those of CW path loading. The coefficient of thermal expansion of PFSA has been reported to be identical in both cooling and heating temperature scans [16]. The differences of strains in these two runs are resulted from the creep behavior in the membrane. It appears that the creep in PFSA material during a temperature change is dependent on temperature history. During the falling temperature, as shown as the step 2 in Fig. 9, the creep was pronounced at the beginning because the membrane was compliant at the initial high temperature. The creep rate started to decrease and even reached to a negative value leading to a small amount of reduce in the creep strain (less than 2%), which was attributed to the changes in the modulus of the material with temperature [17]. As plotted in Fig. 9, during the rising temperature, the creep in step 3 was mild at first and started to accelerate later. However the amount of latter acceleration of creep strains resulted by heating was not comparable to the beginning part of creep during falling temperature as shown in Fig. 9. It can be concluded that the membrane was largely affected by the initial temperature in a variable temperature creep process and this temperature effect on the creep strain would shorten fatigue life of the material [18]. Also, the falling temperature creep strain of the second cycle in CCW path was considerably lower than the first cycle, meaning the effect

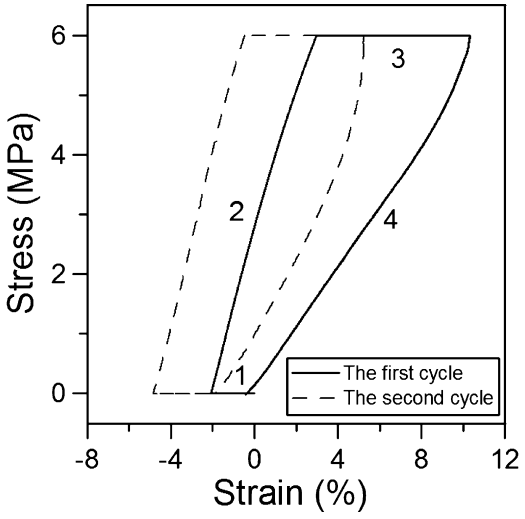

Fig. 8. The stress–strain response of CW rectangular path loading.

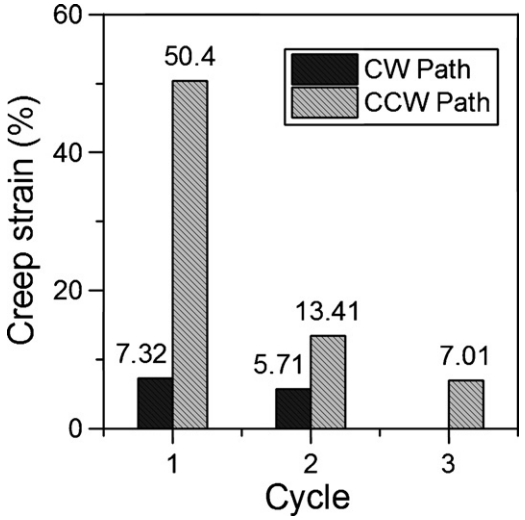

Fig. 10. The comparison of creep in the two kinds of rectangular path loading.

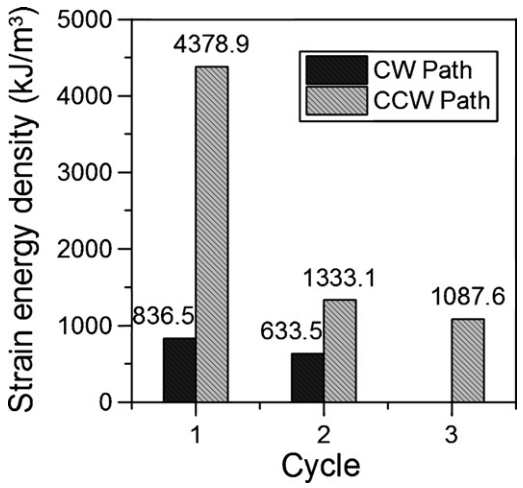

Fig. 11. The comparison of strain energy density in the two kinds of rectangular path loading.

of initial temperature started to equilibrate in sequent loading cycles.

The strain energy density in the first and the second cycle was 836.5 kJ m^{-3} and 633.5 kJ m^{-3} separately in the CW cycles and was much lower than the CCW cycles correspondingly, meaning less plastic deformations was obtained under low temperatures. The comparison of strain energy density in the two kinds of rectangular path loading is shown in Fig. 11. With the analysis of results above, the mechanical responses of the membrane were largely affected by the temperature history. Many properties and behaviors, such as modulus, strain energy density and creep strain were closely related to the temperature loading paths. Therefore, the experiment of temperature cycle is proposed in Section 3.3 in order to study the relation between temperature and thermal stress.

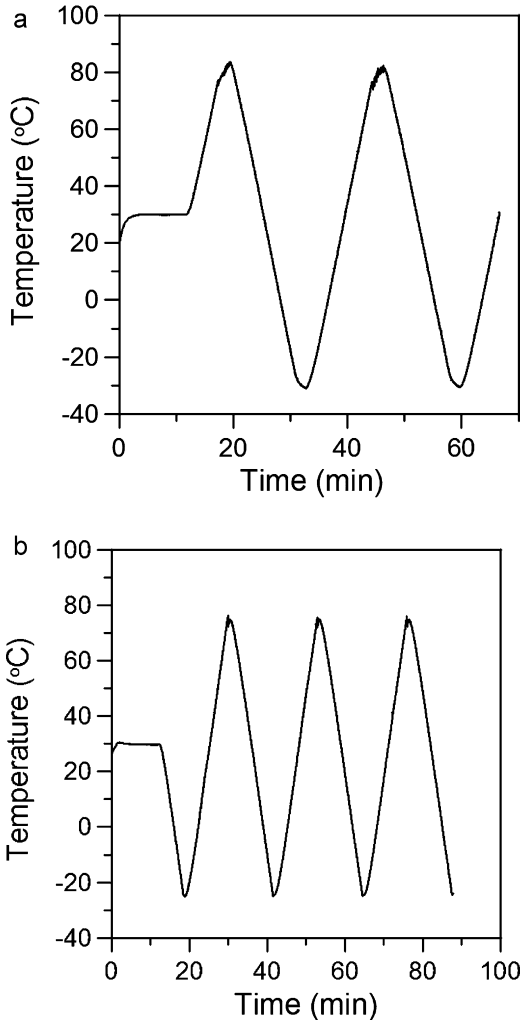

Fig. 12. The paths of temperature cyclic loading: (a) path 1; (b) path 2.

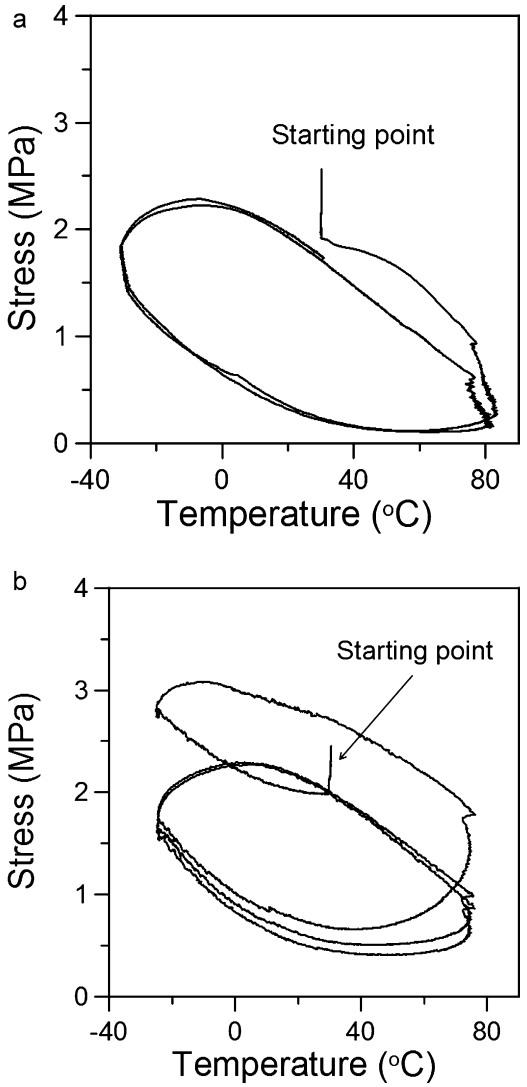

Fig. 13. The thermal stress vs. temperature: (a) path 1; (b) path 2.

3.3. Temperature cyclic tests

The temperature cyclic experiment is to impose thermal loads to the specimen repeatedly. Two types of temperature loading conditions were used here. Cyclic path 1 was elevating the temperature first as shown in Fig. 12(a). Cyclic path 2 was reducing the temperature first as in Fig. 12(b). A small strain (1%) was imposed on the specimen first and no thermal load was applied until the stress caused by the strain was relaxed completely. The point here is to investigate the relationship between thermal load stress and temperature.

The relationship between thermal stresses and temperatures measured in this experiment is plotted in Fig. 13. First of all, the thermal stress hysteresis loop was observed in both two paths.

The stresses were different between heating and cooling processes, indicating a reduced level of stress relaxation [19,20]. Second, it is noteworthy that there was a lag between peaks of temperature cycles and thermal stresses. At the high temperature region, the minimum stress appeared in the cooling part of the curve after passing the highest temperature, where the compensation from relaxation of the stresses to the increasing thermal stresses reached to zero. At the low temperature region, the maximum stresses occurred when the environment was heated back to 0 °C, suggesting the freeze and thaw of the water in the membrane played an important role here. The ice formation kept increasing as long as the temperature was below the freezing point of water and shifted the peak of the thermal stress. During the further part of heating process, stress–temperature curves turned into a straight line after 10 °C. For future notice, the removal of residual water could prevent the damages caused by the phase transition of water during temperature cycling [21].

The relationship between thermal stress and temperature in the two different paths were compared here also. At low temperatures the difference in the stresses for two paths was very small within the temperature range from −30 °C to 20 °C during the heating process and the highest thermal stresses for each path after passing the first high temperature peak were 2.30 MPa and 2.25 MPa respectively, meaning when the membrane was enhanced by freezing and the transition of the polymer, the effect of the initial cooling was very minor. At the high temperature region, stresses in path 2 were higher than path 1. Moreover, the stress–temperature curves overlapped and the specimen reached the steady-state after the first high temperature peak in path 1, while in the path 2 the minimum stress decreased with increasing thermal cycles, meaning the membrane was still in the relaxation of the high thermal stress caused by the initial cooling process.

4. Conclusions

This paper studied the stress–strain response of Nafion® NRE-212 in the case of the interaction of thermal loading and mechanical loading conditions. The thermo-mechanical coupling experiments were conducted following the in-phase proportional path and out-phase rectangular paths (CW and CCW). The effect of thermal loading was also investigated under temperature cyclic loading. Through the analysis of the modulus, strain, strain energy density and other parameters, some conclusions can be drawn as following.

Under the in-phase proportional loading, the deformations of the membrane were resulted from thermal expansion, the cyclic ratcheting strains and creep strain caused by non-zero ambient stress. The membrane reached its equilibrium state right after the first cycle of the test. In the cases of rectangular path loading, the elastic behavior of the membrane at the low temperatures can be explained by the freezing of water content in the material and the transition of the non-ionic matrix. During a variable temperature creep process, the creep strain of Nafion® NRE-212 was history-dependent in the membrane. The effect of initial temperature on the creep has strong influence on the material. In the case of thermal loading, the thermal stress was also history-dependent and a hysteresis was observed. The maximum thermal stress did not occur at the lowest temperature and was shifted by ice formation in the membrane.

In summary, this paper presents an application of thermo-mechanical coupling to PFSA membranes. The presented experimental results indicate that for certain materials, thermo-mechanical coupling during cyclic loading induced interesting mechanical behaviors and can bring further insights into the membrane durability in fuel cell operations. Therefore, such effects should be of interest to the designer and be included in the strength characterization to achieve service life targets [22]. While considering the process gained in this work, a similar study could be performed over a range of relative humilities, providing hygro-thermo-mechanical coupling characterization on PEMs in order to fully understand the behavior of membrane in fuel cell vehicles.

Acknowledgements

The authors gratefully acknowledge financial support for this work from the Program for Changjiang Scholars and Innovative Research Team in University (No: IRT0641) and the Program of Introducing Talents of Discipline to Universities (No: B06006)

References

[1] S.D. Knights, K.M. Colbow, J. St-Pierre, D.P. Wilkinson, Journal of Power Sources 127 (2004) 127–134.
[2] H. Tang, S. Peikang, S.P. Jiang, F. Wang, M. Pan, Journal of Power Sources 170 (2007) 85–92.
[3] L. Wang, Y.Z. Meng, X.H. Li, M. Xiao, S.J. Wang, A.S. Hay, Journal of Membrane Science 280 (2006) 108–115.
[4] Y.H. Lai, D.A. Dillard, in: A.W. Vielstich, H. Gasteiger, H. Yokokama (Eds.), Handbook of Fuel Cells Volume 5: Advances in Electrocatalysis, Materials, Diagnostics and Durability, John Wiley & Sons, Ltd., 2009, pp. 403–419.
[5] K.A. Patankar, D.A. Dillard, S.W. Case, M.W. Ellis, Y.H. Lai, M.K. Budinski, C.S. Gittleman, Mechanics of Time-Dependent Materials 12 (2008) 221–236.
[6] S. Kim, M.M. Mench, Journal of Power Sources 174 (2007) 206–220.
[7] Q. Guo, Z. Qi, Journal of Power Sources 160 (2006) 1269–1274.
[8] R.C. McDonald, C.K. Mittelsteadt, E.L. Thompson, Fuel Cells 4 (2004) 208–213.
[9] E.M. Arruda, M.C. Boyce, R. Jayachandran, Mechanics of Materials 19 (1995) 193–212.
[10] L. Anand, N.M. Ames, V. Srivastava, S.A. Chester, International Journal of Plasticity 25 (2009) 1474–1494.
[11] M.C. Boyce, E.L. Montagut, A.S. Argon, Polymer Engineering and Science 32 (1992) 1073–1085.
[12] ASTM D 882-02, Standard Test Method for Tensile Properties of Thin Plastic Sheeting, American Society for Testing Materials, 2002.
[13] T. Kyu, A. Eisenberg, in: A. Eisenberg, H.L. Yeager (Eds.), Perfluorinated Ionomer Membranes, American Chemical Society, Washington, DC, 1982, p. 79.
[14] K.M. Cable, PhD thesis, University of Southern Mississippi, 1996.
[15] H.W. Starkweather, J.J. Chang, Macromolecules 15 (1982) 752–756.
[16] H.F.M. Mohamed, K. Ito, Y. Kobayashi, N. Takimoto, Y. Takeoka, A. Ohira, Polymer 49 (2008) 3091–3097.
[17] R. Mark, W.N. Findley, Journal of Rheology 22 (1978) 471–492.
[18] W.W. Bose-Filho, E.R. de Freitas, V.F. da Silva, M.T. Milan, D. Spinelli, International Journal of Fatigue 29 (2007) 1846–1854.
[19] M.M. El-Tonsy, Polymer Testing 22 (2003) 57–62.
[20] T. Hanabusa, K. Kusaka, O. Sakata, Thin Solid Films 459 (2004) 245–248.
[21] E. Cho, J.-J. Ko, H.Y. Ha, S.-A. Hong, K.-Y. Lee, T.-W. Lim, I.-H. Oh, Journal of the Electrochemical Society 151 (2004) A661–A665.
[22] Energy USDO, National Hydrogen Energy Roadmap, 2002, http://www1.eere.energy.gov/hydrogenandfuelcells/pdfs/national h2 roadmap.pdf.